Superfluid-to-Solid Crossover in a Rotating Bose-Einstein Condensate

David L. Feder[1,2] and Charles W. Clark[2]

[1]*Institute for Physical Science and Technology, University of Maryland, College Park, Maryland 20742*
[2]*Electron and Optical Physics Division, National Institute of Standards and Technology, Gaithersburg, Maryland 20899-8410*

(Received 31 July 2001; published 17 October 2001)

The properties of a rotating Bose-Einstein condensate confined in a prolate cylindrically symmetric trap are explored both analytically and numerically. As the rotation frequency increases, an ever greater number of vortices are energetically favored. Though the cloud anisotropy and moment of inertia approach those of a classical fluid at high frequencies, the observed vortex density is consistently lower than the solid-body estimate. Furthermore, the vortices are found to arrange themselves in highly regular triangular arrays, with little distortion even near the condensate surface. These results are shown to be a direct consequence of the inhomogeneous confining potential.

DOI: 10.1103/PhysRevLett.87.190401 PACS numbers: 03.75.Fi, 05.30.Jp, 47.37.+q

One of the most striking properties of liquid ^{4}He(II) is its ability to mimic the behavior of a solid body when subjected to uniform rotation. Since the superfluid velocity field $\mathbf{v}_s$ is irrotational ($\nabla \times \mathbf{v}_s = 0$), the superfluid component of ^{4}He(II) might be expected to remain at rest while the normal component rotates with the container. In fact, for sufficiently large values of the rotation frequency Ω, the entire fluid is found to rotate like a classical liquid at all temperatures [1]. The paradox may be resolved by assuming that the superfluid is threaded by quantized vortices. These are singularities of $\mathbf{v}_s$, around which the phase of the superfluid order parameter increases by 2π. Although the mechanisms for the spin-up of the superfluid are not fully understood, at equilibrium the vortices must flow with the normal velocity due to the the mutual friction between superfluid and normal components [2]. In addition to considerable indirect evidence for this hypothesis, small numbers of vortices have been imaged directly in rotating superfluid ^{4}He [3].

In this Letter, we show how the presence of quantized vortices can allow a Bose-Einstein condensate (BEC) to mimic a classical fluid under rotation, as has been suggested by recent experiments at JILA [4]. In these experiments, a trapped gas of ultracold ^{87}Rb atoms is spun up, and then cooled through the Bose-Einstein condensation transition. For small values of Ω, the condensate density is found to assume its usual nonrotating shape, while the thermal cloud bulges outward. This corroborates previous evidence that the condensate behaves as an irrotational superfluid [5,6]. The condensate density profile undergoes a sudden change at a value of Ω that is comparable to the thermodynamic critical frequency for the stability of a single vortex [7]. As Ω increases further, the shape of the condensate gradually approaches that of the thermal cloud. This suggests that, for any given value of Ω and temperature, the condensate contains the appropriate number and distribution of vortices for thermodynamic equilibrium [8]. In contrast, when no appreciable thermal fraction is present, higher rotation frequencies are generally required to nucleate vortices in BECs [9–11].

We present two key results, which also bear on issues raised by recent experiments at MIT [10]. First, the vortices are arranged in extremely regular triangular arrays: Even near the condensate surface, little circular distortion [12] is found. Second, the number of vortices is consistently lower than that required to ensure solid-body rotation throughout the condensate.

To make explicit comparison with the recent JILA experiment, we consider the case of $N = 200\,000$ atoms of ^{87}Rb, confined in a cylindrically symmetric trap with radial frequency $\omega_\rho/2\pi = 8$ Hz, and anisotropy $\lambda \equiv \omega_z/\omega_\rho = \frac{5}{8}$. Unless stated explicitly, our units of energy, angular frequency, length, and time are given by $\hbar\omega_\rho$, ω_ρ, $d_\rho = \sqrt{\hbar/M\omega_\rho} \approx 3.845$ μm, and ω_ρ^{-1}, respectively, where M is the atomic mass and $\hbar$ is Planck's constant h divided by 2π. We work in a frame that rotates with angular frequency Ω about the z axis. The time-dependent Gross-Pitaevskii (GP) equation [13], which governs the dynamics of the condensate wave function ψ of a dilute BEC at zero temperature, is then given by

$$i\partial_t\psi(\mathbf{r},t) = [T + V_{\text{trap}} + V_{\text{H}} - \Omega L_z]\psi(\mathbf{r},t), \quad (1)$$

with kinetic energy $T = -\frac{1}{2}\nabla^2$, trap potential $V_{\text{trap}} = \frac{1}{2}(\rho^2 + \lambda^2 z^2)$, and angular momentum component $L_z = i(y\partial_x - x\partial_y)$. The effects of atomic interactions are included in the nonlinear term $V_{\text{H}} = 4\pi\eta|\psi|^2$, $\eta = Na/d_\rho$, where $a = 5.29$ nm is the scattering length for ^{87}Rb collisions [14]. We use the normalization condition $\int d\mathbf{r}|\psi(\mathbf{r},t)|^2 = 1$. At equilibrium in the rotating frame, $\psi(\mathbf{r},t) = e^{-i\mu t}\psi(\mathbf{r})$, where μ is the chemical potential.

To estimate the properties of a rotating condensate, such as the aspect ratio and the number of vortices, we consider two tractable cases: a single vortex applicable for small Ω, and multiple vortices relevant to high Ω where the condensate is expected to behave essentially as a rigid body.

With one vortex at the center of the trap, $\psi = |\psi|e^{i\phi}$, where ϕ is the polar angle. In the large-N or Thomas-Fermi (TF) limit, the condensate density is $|\psi|^2 = (\mu - \frac{\rho^2}{2} - \frac{\lambda^2 z^2}{2} - \frac{1}{2\rho^2} + \Omega)/4\pi\eta$ when that quantity is positive, and is zero elsewhere [7]. The inner cutoff defines the vortex core size or the healing length ξ; for $\mu \gg 1$, one obtains $\xi \approx 1/\sqrt{2\mu} \sim 1/R_0$, where $R_0 = (15\eta\lambda)^{1/5}$ is the TF radius along $\hat{\rho}$ in the absence of a vortex. A straightforward calculation shows that, for large R_0, the TF radius for an isolated vortex is $R_\rho \approx R_0[1 + (3/2R_0^4)\ln(2R_0/\xi)]$ and the condensate aspect ratio is $\lambda'_{\rm TF} \equiv R_\rho/R_z \approx \lambda[1 + (1/2R_0^2)]$. Assuming this result depends only weakly on vortex position, and is additive with respect to the number of vortices N_v, then in explicit units $\lambda'_{\rm TF} \approx \lambda[1 + \frac{1}{2}N_v(d_\rho/R_0)^2]$ at larger Ω.

For large N_v, as we will show below, the condensate rotates almost as a solid body, so the rotating-frame velocity operator $\mathbf{v}_r = -i\nabla - \Omega\hat{z} \times \mathbf{r}$ can be neglected. Since $T - \Omega L_z = \frac{1}{2}\mathbf{v}_r^2 - \frac{1}{2}\Omega^2\rho^2$, rotation effectively softens the radial potential, $V_{\rm trap} \rightarrow \frac{1}{2}(1 - \Omega^2)\rho^2 + \frac{1}{2}\lambda^2 z^2$. In this case, $R_\rho = R_0/(1 - \Omega^2)^{3/10}$ and $\lambda'_{\rm sb} = \lambda/\sqrt{1 - \Omega^2}$. The number of vortices is the line integral of the phase gradient around the cloud perimeter; assuming the solid-body value of the tangential velocity ΩR_ρ, then the areal vortex density is $n_v = N_v/\pi R_\rho^2 = \Omega/\pi$, and $N_v^{\rm sb} = \Omega R_0^2/(1 - \Omega^2)^{3/5}$.

If the vortices form a regular array at large Ω, then the lattice constant b should be comparable to the average separation between vortices $n_v^{-1/2} \sim \sqrt{\pi/\Omega}$. For a triangular array centered at the origin [15,16], the vortices arrange themselves in concentric hexagonal rings labeled by ring index r, such that $N_v = 1 + 3r(r + 1)$. Assuming the superfluid velocity exactly matches the solid-body value midway between nearest-neighbor vortices (where the two nearest rotational fields exactly cancel), then $N_v = \Omega b^2(r + \frac{1}{2})^2$ and $b \approx \sqrt{3/\Omega}$ for large r. Since $\Omega_{\rm max} = 1$ in a harmonic trap, the smallest vortex separation is $b_{\rm min} \approx \sqrt{3}\, d_\rho$ in explicit units. When the vortex cores begin to overlap significantly ($b \sim \xi$), the system might undergo a phase transition, possibly into a state akin to a quantum Hall insulator [16,17]; since $\xi(\rho = 0, z = 0) = 1/\sqrt{2\mu} = 1/R_0(1 - \Omega^2)^{1/5}$ in the TF limit, the value of Ω for this to occur must become extremely close to unity: $1 - \Omega \sim R_0^{-5}$.

The stationary solutions of the GP equation in the rotating frame, defined as local minima of the free energy $\langle E\rangle = \mu N - \frac{1}{2}\langle V_H\rangle$, are found numerically by norm-preserving imaginary time propagation using an adaptive stepsize Runge-Kutta integrator. The wave function is solved on a three-dimensional Cartesian mesh within a discrete-variable representation [18] based on Gauss-Hermite quadrature, and is assumed to be even under reflection in the $z = 0$ plane. The initial state is taken to be the TF wave function with a phase $\Phi(x, y) = \sum_{x_0,y_0} \tan^{-1}[(y - y_0)/(x - x_0)]$, where (x_0, y_0) are vortex positions in a regular array centered at the origin. The GP equation for a given value of Ω is propagated in imaginary time until the fluctuations in both μ and the norm become smaller than 10^{-11}. The condensate densities integrated down $\hat{x}$ and $\hat{z}$ are then fit to a TF profile using a nonlinear least-squares analysis, where densities lower than 0.1% of the maximum value are discarded. For the vortex-free condensate, this yields an aspect ratio of 0.645, which is 3% larger than the TF value of $\frac{5}{8}$.

The resulting equilibrium configurations are sensitive to the initial vortex distributions. Figure 1 shows three different solutions of the GP equation (1) for $\Omega = 0.45$. These were obtained using seed arrays with rhombohedral (left), square (center), and triangular (right) symmetries, respectively. Though observables such as the energy, angular momentum, and cloud aspect ratio are all comparable, they each have different vortex numbers and arrangements. Though a complete survey of possible configurations is beyond the scope of the present work, for all cases considered the initial rhombohedral vortex distribution is found to yield the final state with lowest energy; for larger Ω, this symmetry gives rise to equilibrium arrays that are generally triangular (see below).

The central results of the present work are shown in Fig. 2, which depicts equilibrium solutions for $0.25 \leq \Omega \leq 0.95$. A single vortex at the origin has appeared by $\Omega = 0.35$; the thermodynamic critical frequency (the energy difference between states with zero and one vortex, divided by $\hbar$) is $\Omega_c = 0.30$. This value is slightly lower than the experimental value $0.32 < \Omega_c < 0.38$; since $\Omega_c \sim N^{-2/5}$, perhaps there are fewer atoms in the condensate at vortex nucleation. (The dynamic critical frequency, at which the first collective mode becomes negative, is somewhat higher: $\Omega_\nu = 0.46$.) With a vortex, the cloud aspect ratio changes to $\lambda = 0.663$; using the fitted values for the nonrotating cloud $\lambda = 0.645$ and $R_0 = 4.86$, the TF prediction is $\lambda'_{\rm TF} = 0.659$. As Ω continues to increase, so does the aspect ratio; the cloud becomes spherical for $0.75 < \Omega < 0.8$ (consistent with the experimental results) and highly oblate for $\Omega = 0.95$, at which $\lambda' = 1.8$.

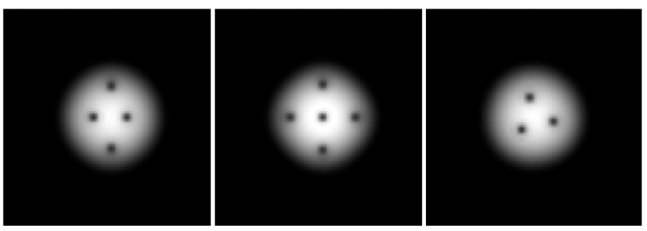

FIG. 1. Three stationary states are shown for $\Omega = 0.45$. From left to right, the values $\{E/N, \mu, \langle L_z\rangle/N\}$ in scaled units are $\{7.20, 11.28, 2.31\}$, $\{7.21, 11.29, 2.33\}$, and $\{7.24, 11.28, 2.19\}$, respectively.

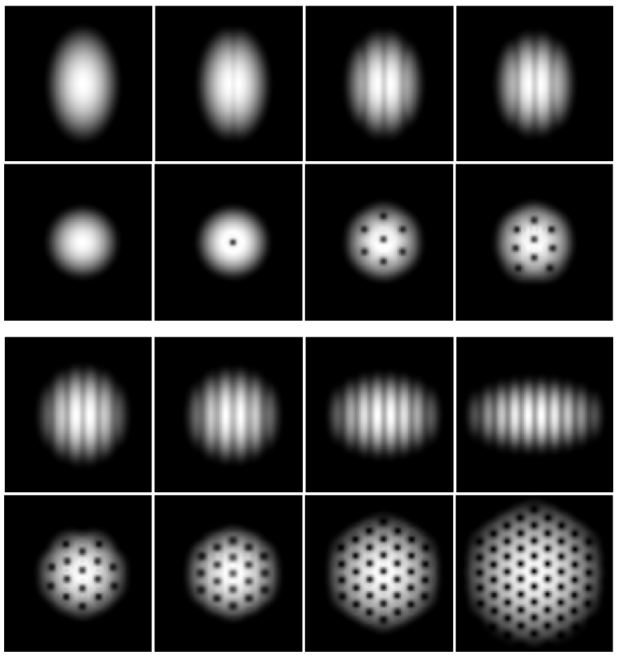

FIG. 2. Condensate densities integrated along $\hat{y}$ (upper row) and $\hat{z}$ (lower row) are shown for $\Omega = 0.25$, 0.35, 0.55, and 0.65 (first data set, left to right) and $\tilde{\Omega} = 0.75$, 0.80, 0.90, and 0.95 (second data set, left to right). Each frame is $20d_\rho \approx 77\ \mu$m on a side.

As shown in Fig. 3, the solid-body estimate of the cloud anisotropy $\lambda'_{\rm sb}$ tracks (but consistently exceeds) our numerical values; in contrast, $\lambda'_{\rm TF}$ is always too small. For example, when $\Omega = 0.95$, one obtains $\lambda'_{\rm sb} = 2.00$ and $\lambda'_{\rm TF} = 1.50$ with $N_v = 65$ (see Fig. 4). The number of enclosed vortices is not known *a priori,* however; using the solid-body estimate $N_v^{\rm sb} = 89$ for $\Omega = 0.95$ yields the much improved $\lambda'_{\rm TF} = 1.83$. Another indication that the condensate is behaving classically at large Ω is the moment of inertia I (inset of Fig. 3). The effective value $I = \langle L_z\rangle/\Omega$ is always lower than the solid-body $I = \langle x^2 + y^2\rangle$, but is within 4% by $\Omega = 0.95$.

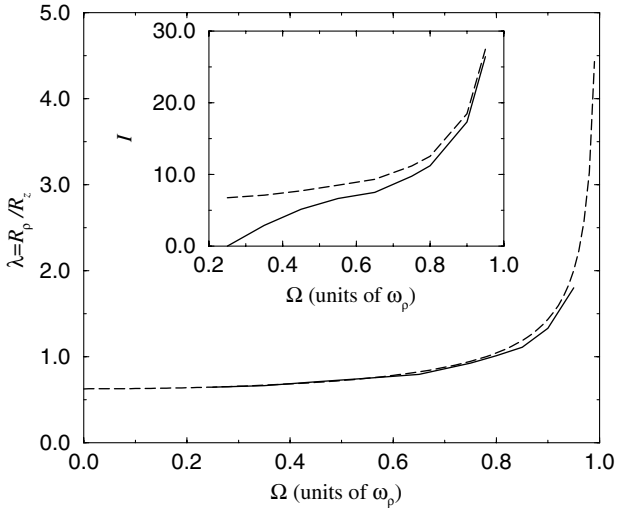

FIG. 3. The cloud aspect ratio $\lambda = R_\rho/R_z$ and moment of inertia I (inset) are shown as a function of rotation frequency Ω. The numerical results (solid lines) for λ are obtained by a TF fit to the cloud profile, and $I \equiv \langle L_z\rangle/N\Omega$. The solid-body (dashed lines) result for the cloud anisotropy corresponds to $\lambda/\sqrt{1-\Omega^2}$, while the corresponding moment of inertia is given by $I = \langle x^2 + y^2\rangle$.

The number of vortices at equilibrium is always considerably lower than the solid-body prediction, as in previous experimental observations [10]. Since the numerical solutions are stationary in the rotating frame, this discrepancy cannot be explained by positing that the vortex array rotates more slowly than the trap. Consider the cases $\Omega = 0.55$, 0.8, 0.9, and 0.95 shown in Fig. 2, which approximate centered triangular arrays with $N_v = 1 + 3r(r+1)$, $r = 1$–4, respectively. The average vortex spacing is found to follow the prediction $b = \sqrt{3/\Omega}$ to within 3%. An additional hexagonal ring of vortices could therefore fit comfortably within the cloud. For $\Omega = 0.95$, $5b = 8.89$ is smaller than the radius $R_\rho = 9.41$, and $r = 5$ corresponds to $N_v = 91$ which is close to the solid-body prediction $N_v^{\rm sb} = 89$. For $N_v = 169$ ($r = 7$), which is comparable to the largest array in experiments at MIT [10], the missing $n_r = 8$ ring implies that the equilibrium number of vortices is of order 20% lower than the solid-body prediction.

The absence of the last ring might be due to the fact that vortices in this low-density region would significantly overlap because of their large core size. Assuming that the vortex diameter is twice the local healing length, then with $\xi(\rho, z=0) = 1/R_\rho\sqrt{(1-\Omega^2)(1-\rho^2/R_\rho^2)}$ one obtains a critical vortex displacement $\rho_c \sim 9$ for $\Omega = 0.95$. In fact, the energy of a uniform array of vortices in a rotating cylinder is also minimized if there exists a "vortex-free strip" the size of approximately one ring near the edge of the vessel [19], i.e., $N_v = 2\pi R^2\Omega/\kappa - \delta$, where $\delta \sim N_v^{-1}$. This correction is due to the contribution to the energy of strictly irrotational flow in the region between the last vortex and the superfluid surface.

The existence of a vortex-free region in trapped condensates is confirmed by evaluating the change in condensate

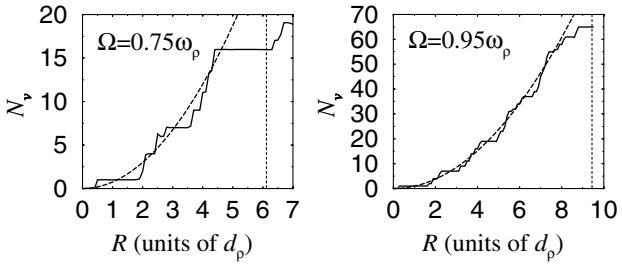

FIG. 4. The number of vortices within a circular contour centered at the origin are shown as a function of contour radius R (solid lines) for $\Omega = 0.75$ and 0.95. The solid-body predictions ΩR^2 (dashed lines) are shown for comparison. The vertical dotted lines denote the TF fit for the radial radius.

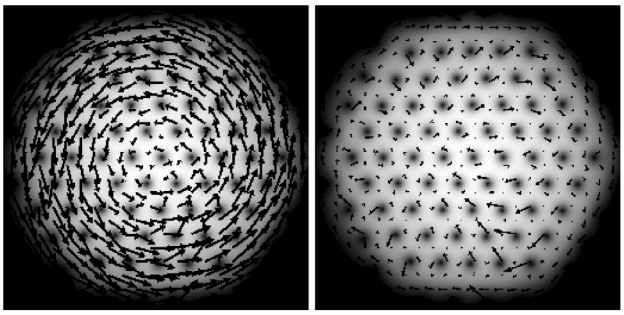

FIG. 5. The velocity field $\mathbf{v}$ in the xy plane is represented by arrows for the $\Omega = 0.95$ case. The left and right images correspond to the laboratory and rotating frames, respectively.

phase around a contour in the xy plane of increasing radius R from the origin. This is accomplished by calculating the spatial derivatives of the numerical data in order to determine $\mathbf{v} \equiv \nabla\Phi$, interpolating the results onto a one-dimensional azimuthal grid with 2000 points, and evaluating the line integral $\oint \mathbf{v} \cdot d\mathbf{l}$ numerically using a trapezoidal rule. The results for $\Omega = 0.75$ and 0.95 are given in Fig. 4. On average, the number of vortices follows the solid-body expression ΩR^2 for small rings, but begins to lag noticeably as $R \rightarrow R_\rho$ even before the vortex-free strip is reached. The velocity field for the $\Omega = 0.95$ case, shown in Fig. 5, is small in the rotating frame everywhere except for the rotational currents near the vortex cores and the irrotational flow near the surface.

In order to further explore this issue, consider a model wave function with constant amplitude and phase given by $\Phi(x, y) = \sum_{x_0,y_0} \tan^{-1}[(y - y_0)/(x - x_0)]$, where (x_0, y_0) are vortex positions in a centered triangular array with lattice constant b. For $N_v = 61$ ($r = 4$), the vortex velocities $v = |\nabla\Phi|$ on successive hexagonal rings n_r are $v = \frac{1}{b}\{3.63, 7.23, 10.69, 13.57\}$. Since $v(n_r = 4) < 4v(n_r = 1)$ by 7%, the angular velocity of the last ring cannot attain the solid-body value for any choice of b. For large arrays, this mismatch in velocities varies as $(R/R_\rho)^5$, and is why significant distortion of the vortex array from triangular is expected near the superfluid surface [12].

The following question immediately arises: Why are the vortex arrays observed in confined condensates so perfectly triangular, even very near the surface? One possible explanation is that a displaced vortex will precess around the origin even in the absence of other vortices, due to the inhomogeneous external potential. Neglecting vortex curvature (which from Fig. 2 is evidently negligible at large Ω), the additional contribution to the velocity is $v = [R/(R_\rho^2 - R^2)]\ln(\xi/R_\rho)$ in the TF limit [7]. Let us return to the case considered above, with $r = 4$, and choose $\Omega = 0.95$ for concreteness. Assuming $R_\rho = R_0/(1 - \Omega^2)^{3/10}$ and imposing $3.63/b + v(R = b) \equiv \Omega b$, one obtains $b = 1.98$ and $v = \{1.88, 3.76, 5.62, 7.37\}$. Thus, including the effect of precession, the solid-body value $v = 4 \times 1.88$ at $R = b$ now exceeds the velocity of the last ring $R = 4b$ by only 2%.

In conclusion, we have explored the crossover of a confined Bose-Einstein condensate from that of an irrotational superfluid to a solid body with increasing rotation. The external potential is shown to strongly influence the density and arrangement of the resulting vortices. Many related issues remain unresolved, however, among them the spin-up of the superfluid by the thermal cloud, the upper critical frequency, and the approach to a quantum Hall state; these will be the subject of future work.

We are grateful to E. A. Cornell and P. C. Haljan for numerous fruitful discussions. This work was supported by the U.S. Office of Naval Research.

[1] D. V. Osborne, Proc. Phys. Soc. London Sect. A **63**, 909 (1950).
[2] I. M. Khalatnikov, *An Introduction to the Theory of Superfluidity* (Benjamin, New York, 1965).
[3] R. J. Donnelly, *Quantized Vortices in Helium II* (Cambridge University Press, Cambridge, England, 1991).
[4] P. C. Haljan, I. Coddington, P. Engels, and E. A. Cornell, cond-mat/0106362.
[5] O. M. Marago *et al.,* Phys. Rev. Lett. **84**, 2056 (2000).
[6] R. Onofrio *et al.,* Phys. Rev. Lett. **85**, 2228 (2000); C. Raman *et al.,* J. Low Temp. Phys. **122**, 99 (2001).
[7] A. L. Fetter and A. A. Svidzinsky, J. Phys. Condens. Matter **13**, R135 (2001).
[8] Y. Castin and R. Dum, Eur. Phys. J. D **7**, 399 (1999).
[9] K. W. Madison, F. Chevy, W. Wohlleben, and J. Dalibard, Phys. Rev. Lett. **84**, 806 (2000).
[10] J. R. Abo-Shaeer, C. Raman, J. M. Vogels, and W. Ketterle, Science **292**, 476 (2001); C. Raman *et al.,* cond-mat/0106235.
[11] E. Hodby *et al.,* cond-mat/0106262.
[12] L. J. Campbell and R. M. Ziff, Phys. Rev. B **20**, 1886 (1979).
[13] E. P. Gross, Nuovo Cimento **20**, 454 (1961); L. P. Pitaevskii, Zh. Eksp. Teor. Fiz. **40**, 646 (1961) [Sov. Phys. JETP **13**, 451 (1961)].
[14] P. S. Julienne, F. H. Mies, E. Tiesinga, and C. J. Williams, Phys. Rev. Lett. **78**, 1880 (1997).
[15] V. K. Tkachenko, Sov. Phys. JETP **22**, 1282 (1966).
[16] T.-L. Ho, Phys. Rev. Lett. **87**, 060403 (2001).
[17] N. R. Cooper, N. K. Wilkin, and J. M. F. Gunn, Phys. Rev. Lett. **87**, 120405 (2001).
[18] B. I. Schneider and D. L. Feder, Phys. Rev. A **59**, 2232 (1999).
[19] H. E. Hall and W. F. Vinen, Proc. R. Soc. London A **238**, 215 (1956).